Buoyancy and polarity driven accumulation of dissolved organic matter in the sea surface microlayer during a phytoplankton bloom

Jasper Zöbelein[1], Shubham Sawle[2], Gernot Friedrichs[2,3], Mariana Ribas-Ribas[1], Carola Lehners[1], Katharina Paetz[1], Maximilian Pflaum[2], Hannelore Waska[1]

[1]Institute for Chemistry and Biology of the Marine Environment (ICBM), School of Mathematics and Science, Carl von Ossietzky Universität Oldenburg, Oldenburg, Germany
[2]Institute of Physical Chemistry, Christian-Albrechts-University Kiel, Kiel, Germany
[3]KMS Kiel Marine Science-Centre for Interdisciplinary Marine Science, Kiel University, Kiel, Germany

Correspondence to: Jasper Zöbelein (jasper.zoebelein@uni-oldenburg.de)

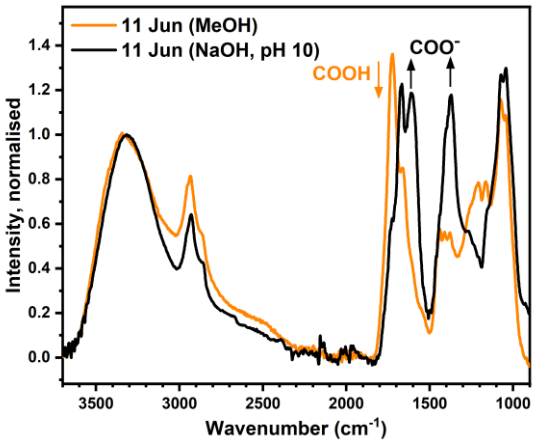

Fig. S1: FTIR spectra of DOM deposits on the ATR crystals from MeOH and NaOH (pH = 10) solution, respectively. For better comparison, the two spectra have been normalised with respect to the maximum of the broad OH/NH bad at 3300 cm^{-1}. As it is outlined in the main text, the very pronounced changes in the spectral signature indicates a high abundance of carboxyl/carboxylate functional groups.

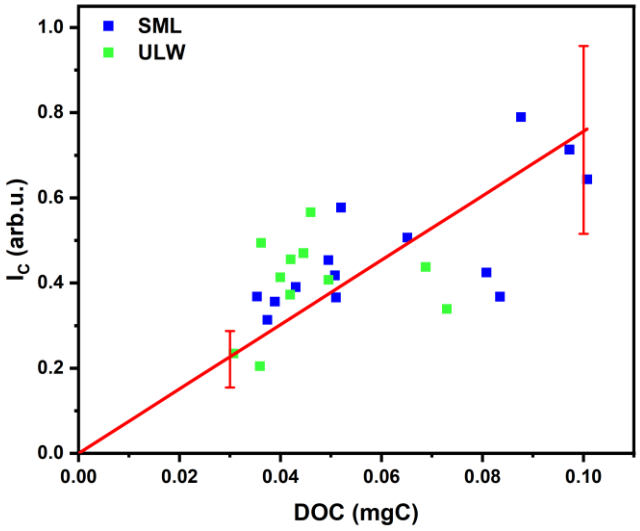

Fig. S2: Correlation between dissolved organic carbon (DOC, mg C in extract) versus integrated ATR-FTIR absorbance of carbon-containing functional groups (I_C; sum of all peak areas, except peaks related to O-H/N-H stretching). The solid line corresponds to a linear fit: $I_C = (7.56 \pm 0.44) \times$ DOC (with fixed intercept, $r = 0.96$, $p < 0.0001$). By using the ratio I_C/m as a mass balance correction factor (see main text), it is implicitly assumed that the scatter in the plot is mainly due to the limited reproducibility of the ATR-FTIR analysis and that the DOC measurement is reliable. The error bars indicate the ±30% (1σ standard deviation) uncertainty of the FTIR measurements from the reference experiments using Triton-X 100. Considering that the experimental data points correspond to the mean of 3-7 individual measurements, the data points exhibit a higher scatter than expected from these reference measurements - presumably indicating the sample-to-sample variability of the DOM pool.

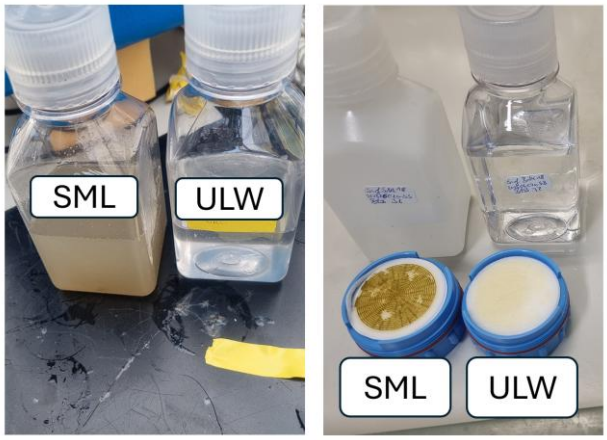

Fig S3: Left: unfiltered samples of SML and ULW during the post-bloom phase. Right: Filters of the same samples showing high amounts of POC accumulating in the SML sample and being removed by filtration.

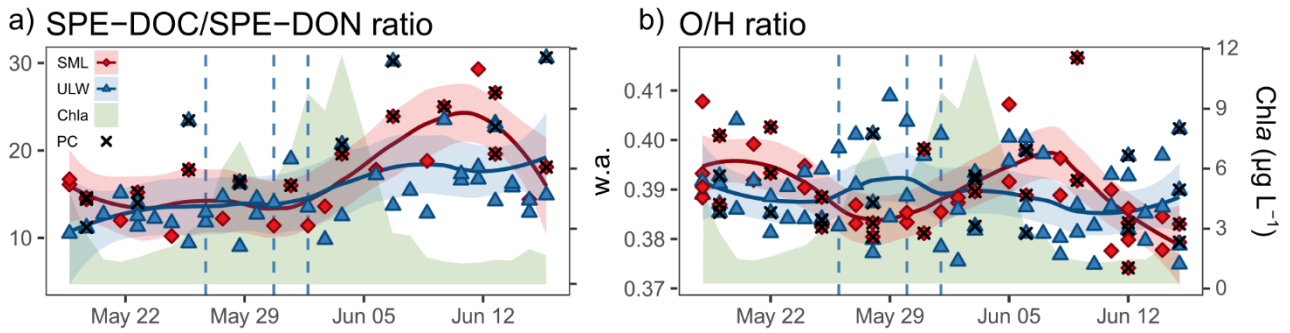

Fig S4: a) Solid-phase extract (SPE)-DOC / DON ratio; b) weighted averaged (w.a.) O/H ratio. SML in red, ULW in blue; the green area indicates Chla development; dotted line indicates nutrient addition; black cross indicates poly carbonate filter, with GFF as default.

Table S1: Selected peak positions with constraing FWHM for spectral decomposition of the ATR-FTIR spectra.

peak no.	peak center (cm^{-1})	constrained FWHM range (cm^{-1})
1	1065	50-200
2	1165	50-100
3	1215	50-100
4	1310	50-300
5	1390	50-200
6	1445	50-200
7	1665	50-200
8	1730	50-200
9	2510	30-500
10	2930	50-500
11	2940	50-100
12	3185	50-500
13	3390	30-500

Table S2: Assignment for the 13 spectrally decomposed ATR-FTIR peaks for SML and ULW DOM samples (Socrates 2001 and listed references).

$\tilde{\nu}$ (cm^{-1})	designation in main text	assignment	typical compound	references
3390, 3185, 2930	**N-H/O-H**	O–H stretch with possible minor N–H "amide A" contribution	alcohols, phenols, amines	Laurson et al. 2020 Pärnpuu et al. 2022 Božič et al. 2018 Yan Ji et al. 2020 Minor et al. 2008
2940	**C-H**	aliphatic C–H stretches (CH_3/CH_2)	fatty acids, lipids/aliphatic, polysaccharides/carbo-hydrates	Rong Lu et al. 2005 Pärnpuu et al. 2022 Minor et al. 2008 Artz et al. 2008
2510	**N-H/O-H**	broad acid O–H envelope tail or aromatic ester	carboxylic acids, aromatic esters	Minor et al. 2008
1730	**C=O**	C=O stretch	carboxylic acids, esters	Artz et al. 2008 Minor et al. 2008
1665	**amide I**	amide I, C=C	proteinaceous compounds, unsaturated lipids	Yan Ji et al. 2020 Minor et al. 2008 Abdulla et. al. 2010
1445, 1390		C-H deformation, OH in- plane bending	aliphatic compounds	Artz et al. 2008 Abdulla et. al. 2010
1309		C–O stretch of aromatic ester/aryl–O or amide III band		Artz et al. 2008 Yan Ji et al. 2020
1215, 1165		C–O stretch, C-O-C	esters, ethers, secondary alcohols	Minor et al. 2008
1065	**C-O/C-O-C**	C–O stretch glycosidic C-O-C	polysaccharides/carbo-hydrates	Pärnpuu et al. 2022 Abdulla et.al 2010 Minor et al. 2008 Artz et al. 2008

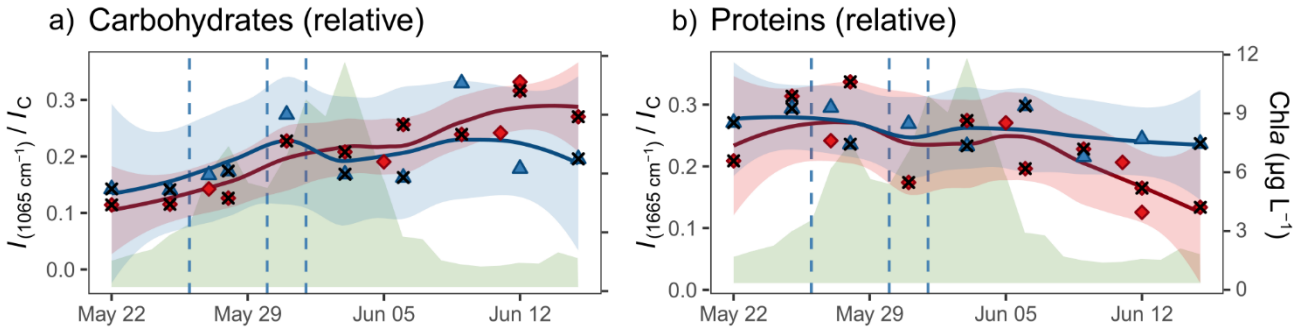

Fig. S5 The relative FTIR spectral intensity trend of the 1065 cm^{-1} band characteristic of carbohydrate-like substances and the 1665 cm^{-1} band characteristic of amide-I stretch vibration in protein-like substances, respectively. SML in red, ULW in blue; the green area indicates Chl*a* development; the dotted line indicates nutrient addition; the black cross indicates a polycarbonate filter, with GFF as default.

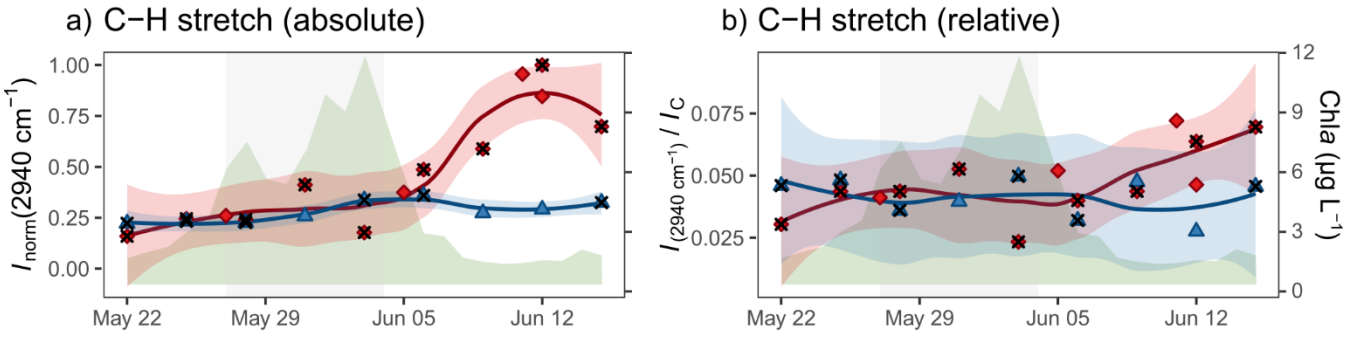

Fig. S6: The absolute and relative spectral intensity trend of the 2940 cm^{-1} band assigned to C-H stretch is highlighted for the SML (red symbols and LOESS trend line) and the ULW (blue symbol and trend line) in panels (a) and (b). The green area indicates Chl*a* development, dotted lines indicate nutrient additions, and black crosses indicate poly carbonate filter extracts, with GFF as default. I_C corresponds to the total integral of carbon-containing functional group peaks.

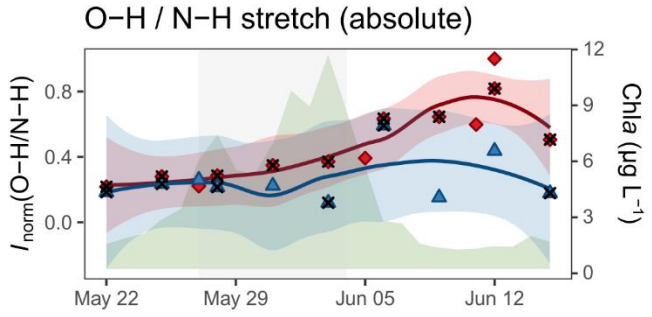

Fig. S7: The absolute intensity trend of the O-H / N-H vibrations (3390, 3185, 2930 and 2510 cm^{-1}) is highlighted for the SML (red symbols and LOESS trend line) and the ULW (blue symbol and trend line) in panel. The green area indicates Chl*a* development, dotted lines indicate nutrient additions, and black crosses indicate poly carbonate filter extracts, with GFF as default.

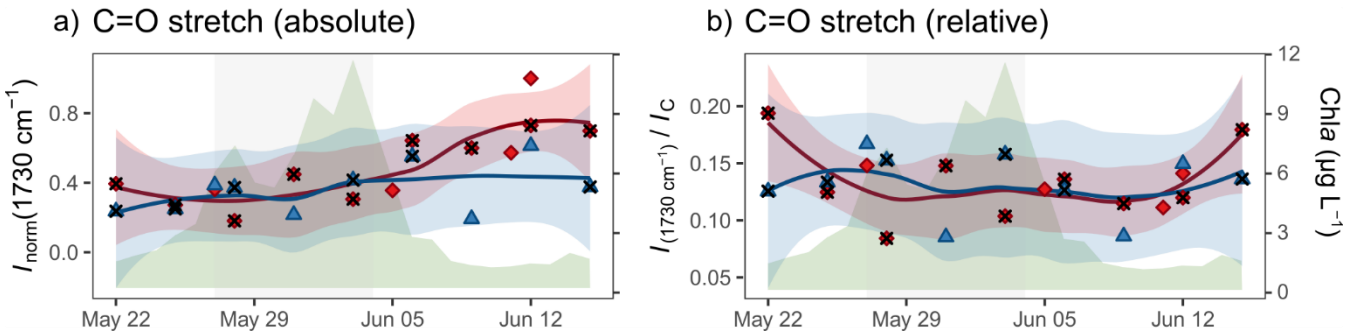

Fig S8: The absolute and relative spectral intensity trend of the 1730 cm^{-1} assigned to carboxylic acid is highlighted for the SML (red symbols and LOESS trend line) and the ULW (blue symbol and trend line) in panels (a) and (b), which is highlighted. The green area indicates Chl*a* development, dotted lines indicate nutrient additions, and black crosses indicate poly carbonate filter extracts, with GFF as default.

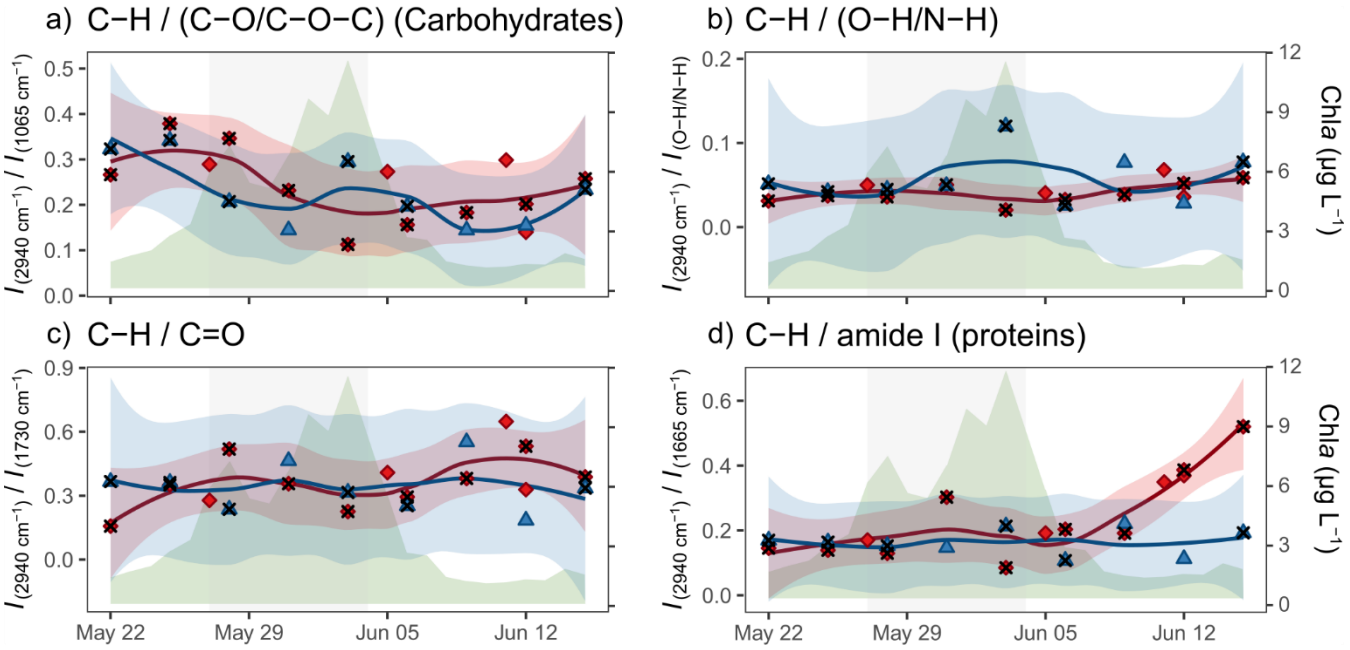

Fig S9 a): FTIR spectral ratio trends for a) Ratios C-H / (C-O / C-O-C) (1065 cm^{-1}) , b) C-H / (O-H / N-H) (3390, 3185, 2930, 2510 cm^{-1}), c) C-H / C=O (1730 cm^{-1}) and d) C-H / amide I (1665 cm^{-1}). SML in red, ULW in blue; the green area indicates Chl*a* development; dotted line indicates nutrient addition; black cross indicates poly carbonate filter, with GFF as default.

Tab. S3: DOM characteristics of mesocosm study samples during the bloom phases as well as reference values for natural water samples.

Origin	Depth	H/C (w.a.)	O/C (w.a.)	I_{DEG}	MLB_{wL}	AI_{mod} (w.a.)	I_{bio}	I_{photo}	Carbo-hydrate-like (w.a. %)	Lipid-like (w.a. %)
pre-bloom	SML	1.20	0.46	0.52	5.87	0.29	0.54	0.36	0.33	0.07
	n=14	±0.01	±0.01	±0.05	±0.39	±0.01	±0.05	±0.02	±0.09	±0.03
	ULW	1.20	0.45	0.53	5.83	0.29	0.52	0.36	0.32	0.07
	n=24	±0.01	±0.01	±0.04	±0.37	±0.00	±0.05	±0.02	±0.10	±0.04
	t-test / p-value	0.63	0.91	0.69	0.76	0.5	0.46	0.65	0.68	0.8
bloom	SML	1.21	0.45	0.51	7.08	0.28	0.53	0.35	0.56	0.12
	n=15	±0.00	±0.01	±0.03	±0.42	±0.00	±0.02	±0.02	±0.10	±0.04
	ULW	1.20	0.46	0.52	6.60	0.29	0.53	0.34	0.51	0.08
	n=22	±0.01	±0.01	±0.04	±0.43	±0.01	±0.02	±0.02	±0.14	±0.02
	t-test / p-value	0.04 *	0.32	0.52	0.0017 **	0.24	0.56	0.65	0.23	0.0011 **
post-bloom	SML	1.22	0.46	0.48	8.83	0.27	0.57	0.31	1.06	0.14
	n=16	±0.01	±0.01	±0.05	±0.89	±0.01	±0.05	±0.02	±0.29	±0.03
	ULW	1.22	0.46	0.46	7.71	0.28	0.56	0.30	0.64	0.10
	n=26	±0.01	±0.01	±0.06	±0.51	±0.00	±0.07	±0.03	±0.26	±0.04
	t-test / p-value	0.17	0.76	0.39	<0.001 ***	0.072	0.66	0.44	<0.001 ***	0.005 **
[1]Mid-Bay	SML	1.44 ±0.41	0.295 ±0.20							
	ULW	1.50 ±0.40	0.332 ±0.22							
[2]Upper estuary	SML	1.23	0.46	0.21						
	ULW	1.22	0.45	0.20						
[2]Middle estuary	SML	1.25	0.47	0.23						
	ULW	1.23	0.47	0.20						
[2]Marine station	SML	1.27	0.48	0.21						
	ULW	1.25	0.49	0.17						
[3]North SW				0.63 ±0.01	11.9 ±0.8					
[4]North SW		1.26 ±0.01	0.40 ±0.03		12	0.28 ±0.02				
NEqPIW	n=6	1.26 ±0.00	0.46 ±0.00	0.84 ±0.01	4.69 ±0.12	0.23 ±0.00	0.02 ±0.01	0.27 ±0.02	0.14 ±0.02	0.02 ±0.12

Averages (± standard deviation) were calculated from experimental replicates

p-value significance: * (< 0.05), ** (< 0.01), and *** (< 0.001)

North SW North Sea seawater, *NEqPIW* North Pacific Equatorial Intermediate Water

[1]Burdette et al. (2022), June 2019. Quadrupole time-of-flight MS data (qToF-MS)

[2]Lechtenfeld et al. (2013), May 2009

[3]Waska and Banko-Kubis (2024), June 2020

[4]Amoako et al. (2025), October 2022

References

Abdulla, H. A. N.; Minor, E. C.; Dias, R. F.; Hatcher, P. G. Changes in the compound classes of dissolved organic matter along an estuarine transect: A study using FTIR and ^{13}C NMR. *Geochim. Cosmochim. Acta* **2010**, *74* (13), 3815–3838. https://doi.org/10.1016/j.gca.2010.04.006

Amoako, K., Reckhardt, A., Roberts, M., Meyer, R., Brick, S., Dittmar, T., Waska, H., 2025. Organo-mineral interactions modulate organic carbon retention and mobility in a deep subterranean estuary of a high-energy beach. Front. Water 7. https://doi.org/10.3389/frwa.2025.1507564

Artz, R. R. E.; Chapman, S. J.; Robertson, A. H. J.; Potts, J. M.; Laggoun-Défarge, F.; Gogo, S.; Comont, L.; Disnar, J.-R.; Francez, A.-J. FTIR spectroscopy can be used as a screening tool for organic matter quality in regenerating cutover peatlands. *Soil Biol. Biochem.* **2008**, *40* (2), 515–527. https://doi.org/10.1016/j.soilbio.2007.09.019

Božič, M.; Elschner, T.; Tkaučič, D.; Bračič, D.; Bračič, M.; Hribernik, S.; Stana-Kleinschek, K.; Kargl, R. Effect of different surface-active polysaccharide derivatives on the formation of ethyl cellulose particles by the emulsion–solvent evaporation method. *Cellulose* **2018**, *25*, 6901–6922. https://doi.org/10.1007/s10570-018-2062-2

Burdette, T.C., Bramblett, R.L., Deegan, A.M., Coffey, N.R., Wozniak, A.S., Frossard, A.A., 2022. Organic Signatures of Surfactants and Organic Molecules in Surface Microlayer and Subsurface Water of Delaware Bay. ACS Earth Space Chem. 6, 2929–2943. https://doi.org/10.1021/acsearthspacechem.2c00220

Ji, Y.; Yang, X.; Ji, Z.; Zhu, L.; Ma, N.; Chen, D.; Jia, X.; Tang, J.; Cao, Y. DFT-calculated IR spectrum amide I, II, and III band contributions of N-methylacetamide fine components. *ACS Omega* **2020**, *5* (15), 8572–8578. https://doi.org/10.1021/acsomega.9b04421

Laurson, P.; Raudsepp, P.; Kaldmäe, H.; Kikas, A.; Mäeorg, U. The deconvolution of FTIR-ATR spectra to five Gaussians for detection of small changes in plant–water clusters. *AIP Adv.* **2020**, *10* (8), 085214. https://doi.org/10.1063/5.0011700

Lechtenfeld, O.J., Koch, B.P., Gašparović, B., Frka, S., Witt, M., Kattner, G., 2013. The influence of salinity on the molecular and optical properties of surface microlayers in a karstic estuary. Marine Chemistry 150, 25–38. https://doi.org/10.1016/j.marchem.2013.01.006

Lu, R.; Gan, W.; Wu, B.-H.; Zhang, Z.; Guo, Y.; Wang, H.-F. C–H stretching vibrations of methyl, methylene, and methine groups at the vapor/alcohol (n = 1–8) interfaces. *J. Phys. Chem. B* **2005**, *109* (29), 14118–14129.

Minor, E. C.; Stephens, B. Dissolved organic matter characteristics within the Lake Superior watershed. *Org. Geochem.* **2008**, *39* (11), 1489–1501. https://doi.org/10.1016/j.orggeochem.2008.08.001

Pärnpuu, S.; Astover, A.; Tõnutare, T.; Penu, P.; Kauer, K. Soil organic matter qualification with FTIR spectroscopy under different soil types in Estonia. *Geoderma Reg.* **2022**, *28*, e00483. https://doi.org/10.1016/j.geodrs.2022.e00483

Socrates, G. *Infrared and Raman Characteristic Group Frequencies: Tables and Charts*, 3rd ed.; John Wiley & Sons: Chichester, 2001.